Available online at www.sciencedirect.com
SCIENCE DIRECT
Polymer 46 (2005) 1967–1981
polymer
www.elsevier.com/locate/polymer

Roll-drawing and die-drawing of toughened poly(ethylene terephthalate). Part 2. Fracture behaviour

J. Mohanraj[a], N. Chapleau[b], A. Ajji[b], R.A. Duckett[a], I.M. Ward[a,*]

[a]*School of Physics and Astronomy, University of Leeds, Leeds, UK*
[b]*Industrial Materials Institute—NRC, Boucherville, Quebec, Canada*

Received 1 March 2004; received in revised form 23 August 2004; accepted 14 October 2004
Available online 25 January 2005

Abstract

Orientation of polymers in the solid-state has been used for a long time in enhancing the properties of the products and the die-drawing process at Leeds University (UK) and the roll-drawing process at IMI (Canada) have been used to produce oriented polymer products in a wide variety of shape and sizes. In this work, we explore the fracture behaviour of isotropic and oriented toughened poly(ethylene terephthalate) (PET) in order to improve the toughness of the oriented products in a direction other than the principal draw direction.

The fracture behaviour of isotropic and oriented PET homopolymer and the two PET blends (containing 10% polyethylene elastomer and 10% compatibilized elastomer) was studied using the multi-specimen *J*-integral approach. In the isotropic case, the compatibilized blend had higher toughness than the homopolymer and the non-compatibilized blend. The oriented sheets from the die-drawing and roll-drawing process, drawn to a draw ratio of 3.2 at 170 °C were tested with the initial notch both parallel and perpendicular to the draw direction. For the former case, the compatibilized blend was tougher and in the other direction the drawn homopolymer was tougher than the blends. At similar draw ratios, the fracture behaviour and the toughness of the oriented sheets from the die-drawing and roll-drawing processes were identical.

Keywords: Toughened PET; Oriented polymers; Fracture toughness

1. Introduction

The demand for polymeric materials in major structural applications has highlighted the need for improving the stiffness and toughness of these materials. This led to the development of innovative solid-state orientation processes such as hydrostatic extrusion, die-drawing, roll-drawing etc., where the polymers are oriented below their melting regime in the case of semi-crystalline polymers and above the glass transition temperature for amorphous polymers. Molecular orientation causes a high level of property enhancement in the oriented products in the draw direction but, in general, the toughness other than in the principal draw direction reduces with draw ratio [1].

It has been well established that by dispersing moderate amounts of a well-defined elastomer phase in the polymer matrix, the toughness can be significantly improved [2–5]. These inclusions alter the stress state in the material and induce extensive plastic deformation in the matrix by the way of multiple crazing and/or shear yielding of the matrix [6–9]. In part 1 of this series, we reported the production, properties, morphology and structure of highly oriented semi-crystalline poly(ethylene terephthalate) (PET) homopolymer and blends obtained by the roll-drawing and the die-drawing processes. The objective of the present work is to study the fracture behaviour of isotropic and oriented toughened PET obtained from the roll-drawing and the die-drawing processes. The oriented materials from the roll-drawing and the die-drawing processes will be tested parallel and perpendicular to the orientation direction and their behaviour will be compared to the isotropic case.

Much of the previous research has concentrated on studying the fracture behaviour of amorphous PET [10–12].

* Corresponding author. Tel.: +44 113 3433808; fax: +44 113 3433809.
E-mail address: i.m.ward@leeds.ac.uk (I.M. Ward).

0032-3861/$ - see front matter © 2004 Elsevier Ltd. All rights reserved.
doi:10.1016/j.polymer.2004.10.090

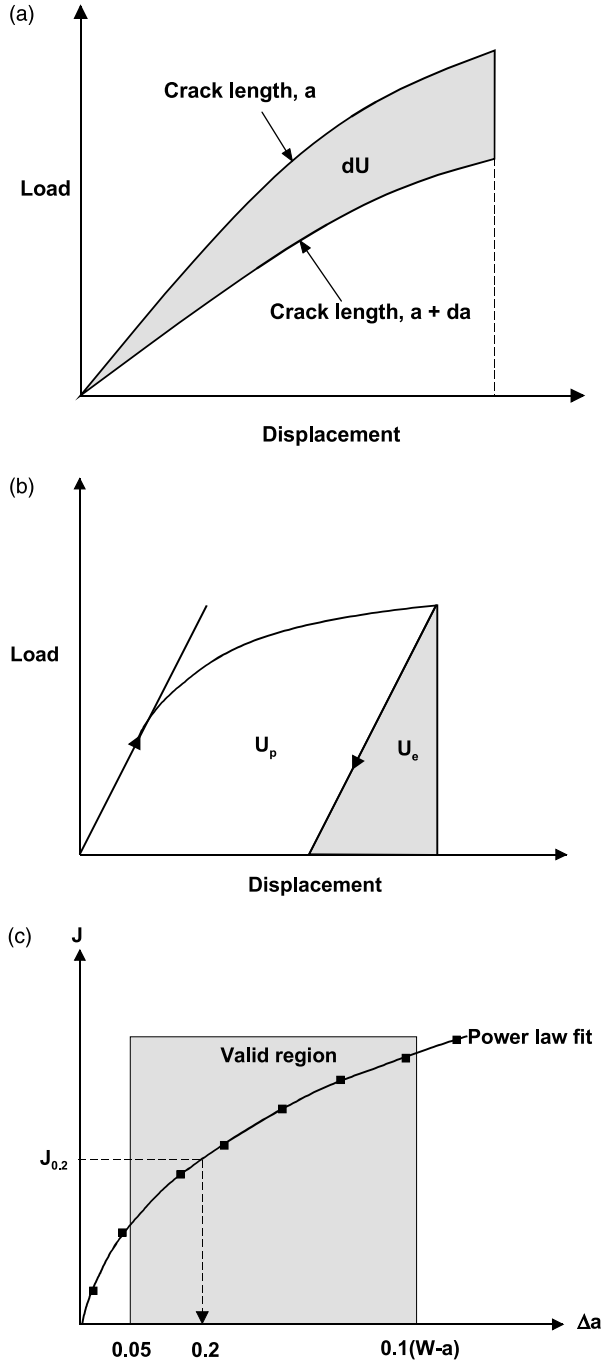

Fig. 1. (a) Non-linear load-displacement curves for two specimens with different crack lengths, a and $(a+\mathrm{d}a)$. (b) Partitioning the total energy into elastic (U_e) and plastic (U_p) components. (c) Schematic representation of a J-Δa curve according to ASTM D6068:96 standard.

Very little has been reported on the fracture of semi-crystalline PET. Fracture studies on semi-crystalline PET were first initiated by Stearne and Ward [13] and later developed by Foot and Ward [14,15], who observed that in semi-crystalline PET, fracture occurred by inherent flaws between amorphous and crystalline boundaries. Pecorini and Hertzberg [16] studied the effect of annealing and drying conditions on the fracture and fatigue behaviour of PET and correlated their results qualitatively to the changes in the tie-molecule density.

For tough polymers or for cases where the plane-strain conditions cannot be maintained at the crack tip, linear elastic fracture mechanics parameters—K_C and G_C—cannot be used to characterize the fracture behaviour because of the large plastic deformations. For these cases, three approaches have been widely used to characterize the fracture behaviour: the J-integral, the crack opening displacement (COD) and the essential work of fracture (EWF). One condition for the validity of results analysed by the EWF theory is that the effective ligament should yield prior to crack propagation [17], i.e. total plane-stress conditions have to be observed in the ligament. In other words, the failure should occur by ductile tearing of the yielded and necked ligament region and the maximum stress reaches a steady state that may be either above or below the criterion predicted according to Hill's plasticity theory [18]. In the present case, initial experiments were performed on semi-crystalline PET homopolymer to check the validity of the EWF methodology. It was found from these initial tests that the samples under quasi-static loading conditions exhibited a mixed mode fracture, in plane-strain and plane-stress conditions, i.e. the crack propagation started before the ligament yielded completely. As the conditions for the validity of the EWF approach were not fulfilled, it was decided to employ the J-integral approach for the present study. This technique has been found to be successful for a wide variety of polymers and toughened polymers that exhibited plastic flow at the crack tip, either under quasi-static loading [19–35] or impact loading conditions [36–43], before fracture.

1.1. J-integral concept

The J-integral is defined as the difference in potential energy between two identical bodies of different crack lengths at constant Δ as shown in Fig. 1(a) and given by [44];

$$J = -\left(\frac{1}{B}\frac{\mathrm{d}U}{\mathrm{d}a}\right)_{\Delta} \tag{1}$$

where B is the thickness of the loaded body, $\mathrm{d}U$ is the difference in potential energy between two loaded bodies with crack lengths, a and $(a+\mathrm{d}a)$.

Sumpter and Turner [45] expanded the above equation in terms of an elastic part J_e and plastic part J_p, such that:

$$J = J_e + J_p \tag{2}$$

$$J = \frac{\eta_e U_e}{B(W-a)} + \frac{\eta_p U_p}{B(W-a)} \tag{3}$$

where U_e and U_p are the elastic and plastic components of the total energy, U (Fig. 1(b)), η_e and η_p are their corresponding geometrical correction factors and a and W

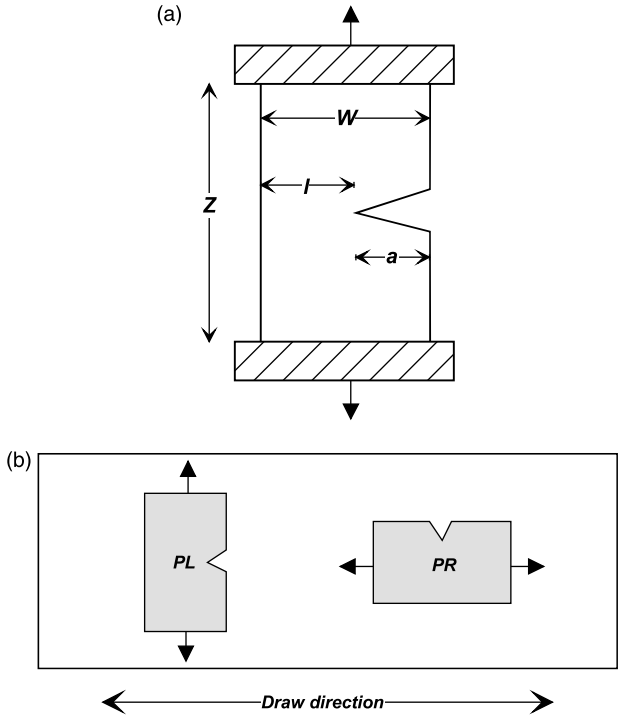

Fig. 2. (a) Schematic diagram showing the single edge notch tension (SENT) geometry used for the *J*-integral measurements. (b) Orientation of the SENT sample with respect to the draw direction.

are the initial crack length and width of the test sample. For the single edge notch tension (SENT) geometry [32]:

$$\eta_e = \frac{(W-a)Y^2a}{\int\left(Y^2a\,da + \frac{Z}{2W}\right)} \tag{4}$$

$$\eta_P = \frac{(W-a)}{W\alpha\left[\left(\frac{W-a}{W[\alpha-(a/W)]}\right)+1\right]^{-1}} \tag{5}$$

where $\alpha = [1-2(a/W)+2(a/W)^2]^{1/2}$, $Y = 1.99-0.41(a/W)+18.70(a/W)^2-38.48(a/W)^3+53.84(a/W)^4$ and Z is the gauge length of the test sample.

Choosing a/W of 0.48 for the SENT geometry would give a value of η_e and η_p to be 2.4 which reduces Eq. (3) to

$$J = \frac{2.4}{B(W-a)}(U_e+U_p) = \frac{2.4}{B(W-a)}(U) \tag{6}$$

where U is the total energy under the load-displacement curve.

Initial assessment of the fracture behaviour favoured the ASTM D6068:96 approach (multi specimen $J_{0.2}$ scheme) to be more suitable for the PET systems used in this study. The semi-circular crack front due to the mixed stress-state condition in the sample, together with the opacity appearance of the sample, made the precise initiation point difficult to determine during the test, which is required in other *J*-integral techniques. Although the single specimen technique proved to be advantageous in terms of conservation of time and material, the error associated with the calculated J_C value was substantial. Hence this approach was not followed in the present case. Thus the elastic fracture mechanics based on the multi specimen *J*-integral approach was employed to measure the toughness of the isotropic and oriented PET homopolymer and the blends. In this method, identical specimens having the same crack length to width ratio are loaded monotonically to various values of crack extension and then unloaded. According to the ASTM protocol [46], the critical *J*-value (J_C) was defined as the intersection of the *J* vs. Δa power law curve, defined by two exclusion lines at 0.05 mm and 10% of

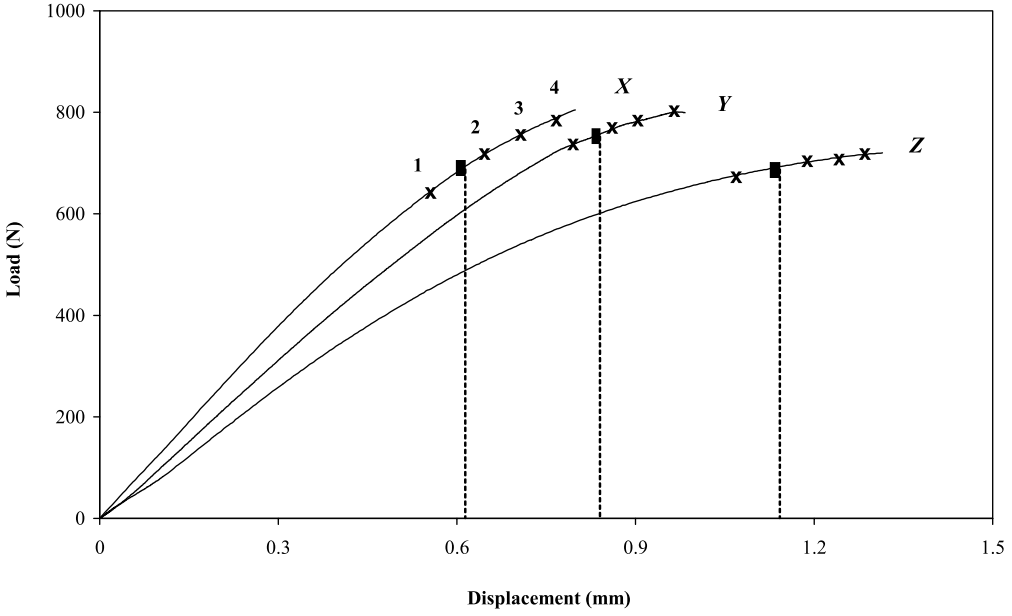

Fig. 3. Load-displacement plots with crack initiation points (■) for isotropic X (PET), Y (10 wt% mPE) and Z (10 wt% GMA-mPE).

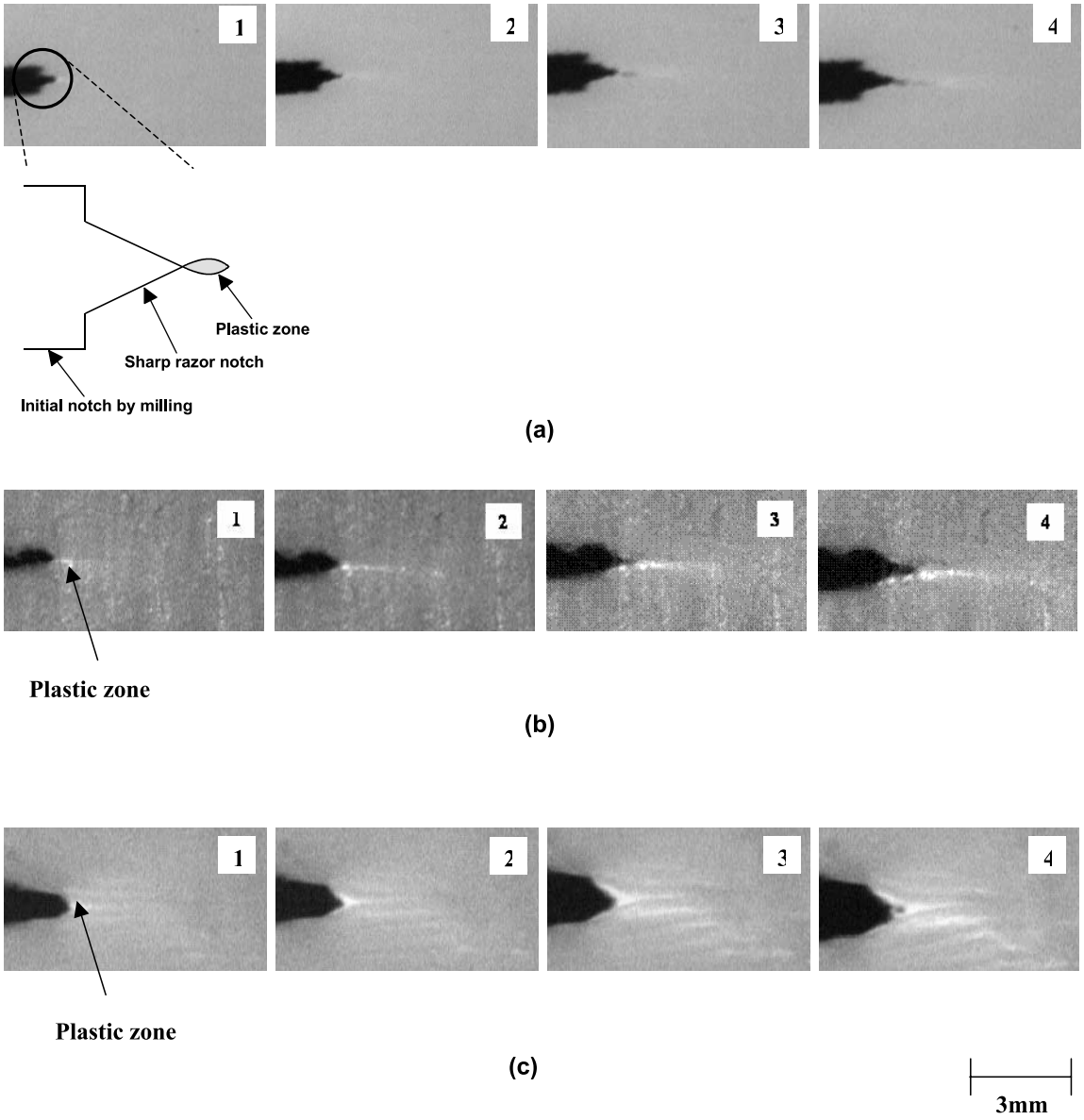

Fig. 4. Photographic sequence during the SENT test for isotropic (a) X (PET), (b) Y (10 wt% mPE) and (c) Z (10 wt% GMA-mPE). 1–4 in the inset of the photographs correspond to the points marked on the load-displacement curve shown in Fig. 3.

the original uncracked ligament length drawn parallel to the *Y*-axis, with an offset line drawn parallel to the *Y*-axis at $\Delta a = 0.2$ mm, i.e.

$$J_{0.2} = C_1(0.2)^{C_2} \tag{7}$$

where C_1 and C_2 are the power law constants. A schematic sketch of the J vs. Δa curve for the calculation of $J_{0.2}$ value using the ASTM standard is shown in Fig. 1(c). Although there is no theoretical justification for choosing the J value at 0.2 mm crack growth, it has been accepted to be universal for quoting the toughness of polymers.

2. Experimental

2.1. Materials

Three materials were investigated in this study. They are X—PET homopolymer, Y—PET + 10% by weight non-grafted elastomer and Z—PET + 10% by weight grafted elastomer. The PET used in this study was a commercial grade polymer, Cleartuf 8006 from Shell. The elastomer blended with the PET was Engage 8150 elastomer (mPE) manufactured by Dow-DuPont. Engage 8150 elastomer is an ethylene–octene copolymer containing 25% octene. In the case of material Z, the elastomer was grafted with

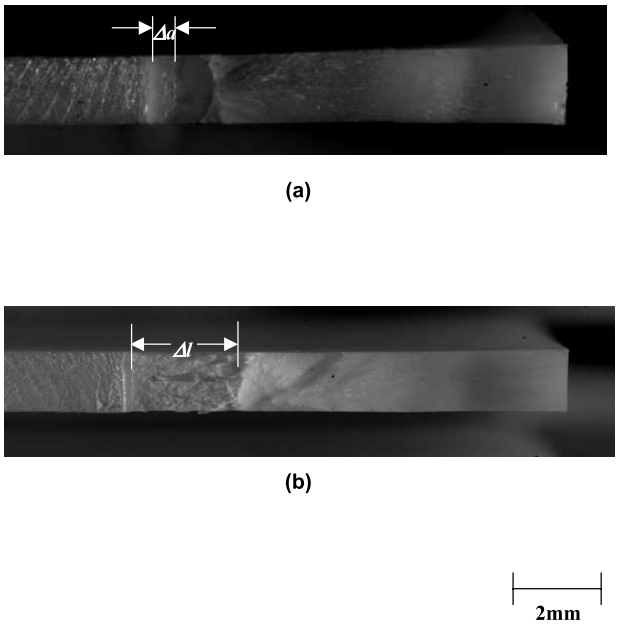

Fig. 5. Fracture surface of isotropic (a) X (PET) and (b) Y (10 wt% mPE) after the SENT test. Δa = crack extension and Δl = length of the stress-whitened zone.

glycidyl methacrylate (GMA) before blending with PET, to investigate the effect of interfacial adhesion.

The blends were compounded in a co-rotating twin-screw extruder, at 290 °C and 200 rpm, and pelletized. From pellets, sheets of approximately 5 mm thick and 100 mm wide were extruded at 290 °C. The extruded sheets were used as the start-up material for die-drawing and roll-drawing.

The roll-drawing and the die-drawing processes are described in detail in part 1 of this series. For this work, PET homopolymer (X) and the blends (Y and Z) were drawn at 170 °C to yield an actual draw ratio (draw ratio in the axial direction) of 3.2.

2.2. Fracture tests

For fracture tests on isotropic sample, single edge notch tensile (SENT) specimens (Fig. 2(a)) of nominal dimensions $60\times20\times2$ mm^3 were machined from the extruded sheet. Initial notches were made by using a slitting saw and the root tips were sharpened by pressing a fresh razor blade into the tip. The oriented sheets, die-drawn and roll-drawn to a draw ratio of 3.2 at 170 °C, were tested both parallel (PL) and perpendicular (PR) to the draw direction as shown in Fig. 2(b). The tests were performed in the Instron tensile testing machine at a crosshead speed of 0.1 mm/min in a temperature-controlled room maintained at 20 °C. The load-displacement data were recorded onto a computer equipped with software to compute the area under the load-displacement curve. The deformed samples were quenched in liquid nitrogen for 10 min and fractured at high speed. The initial crack length (a) and the crack growth (Δa) or, in some cases, the length of the stress-whitened zone (Δl), was measured from the broken surfaces using a travelling microscope.

3. Results and discussion

3.1. Fracture behaviour of isotropic X, Y and Z

The load-displacement plots for isotropic X (PET), Y (10 wt% mPE) and Z (10 wt% GMA-mPE) and the photograph of the crack tip at specific points during the SENT test are shown in Figs. 3 and 4, respectively.

In the case of X, the blunting of the crack tip occurred in the linear portion of the load-displacement curve. A very small plastic zone, confined to the crack tip, was visible in this linear region (Fig. 4(a-1)). On further loading to point 2, the curve deviated from the linear regime and the crack growth occurred at the tip of the notch (Fig. 4(a-2)) and propagated into the damage zone. At point 3 on the load-displacement curve, the main crack appeared to be stopped and a secondary crack initiated and grew ahead of the main propagating crack leaving an island of material in between as shown in Fig. 4(a-3). The two cracks coalesced at point 4 and, at this stage, another crack can be seen to initiate and propagate ahead of this main crack. The fracture process is reminiscent of the discontinuous crack growth in polyethylene tested under constant load conditions [47,48]. Lu et al. [47] attributed the discontinuous growth phenomena to the formation of a fibrillar region between the primary and secondary cracks. Further loading to point 4 weakened the fibrils due to disentanglement of the chains and ultimately, at this point, the fibrillar regions rupture resulting in coalescence of the two cracks (Fig. 4(a-4)).

In the case of blend Y (10 wt% mPE), a plastic zone, visible by naked eye, just formed ahead of the crack tip when the curve deviated from the linear region. As a result of this plastic zone, the crack tip appeared blunted (Fig. 4(b-1)). On further loading, the plastic zone propagated further ahead of the crack tip and the material in this region was pulled in. The white marks on the photographs are reflections from the surface. The stable crack growth started at point 2 (Fig. 4(b-2)) and travelled henceforth in the yielded zone (Fig. 4(b-3) and (b-4)).

In material Z (10 wt% GMA-mPE), the crack tip was shallower than that of blend Y and the plastic zone, ahead of the crack tip, was more diffuse (Fig. 4(c)). This is clearly different from that seen in the case of blend Y, where the plastic deformation was highly localized only at the crack tip (Fig. 4(b)). The diffuse stress whitened zones could be possibly due to cavities in the elastomer and crazing of the matrix at higher strains. The crack growth occurred by the tearing of the yielded material.

The thumbnail shaped crack growth (Δa) was clearly visible on the fracture surface for isotropic X after the high-speed cryogenic fracture as shown in Fig. 5(a). Next to the crack front, a smooth surface appeared probably due to the

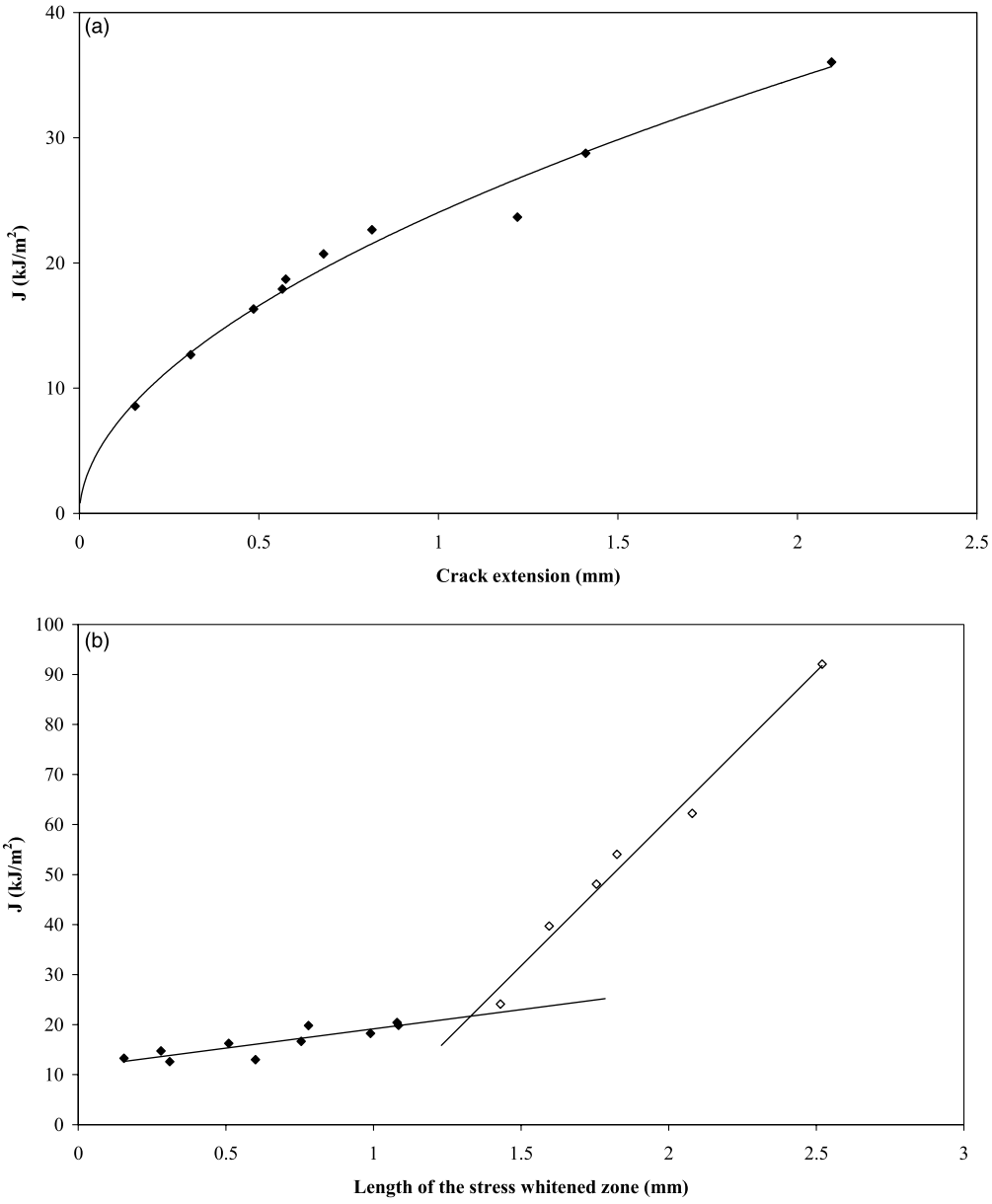

Fig. 6. (a) J vs. Δa curve for isotropic X (PET). (b) J vs. Δl curve for isotropic Y (10 wt% mPE). (c) J vs. Δl curve for isotropic Z (10 wt% GMA-mPE).

initiation of the natural crack during the high-speed cryogenic fracture. In the case of the toughened blends Y and Z, after the deformed samples were fractured in liquid nitrogen, the observations on the fracture surface showed no evidence of the crack front because of the ductility on the fracture surface as shown in Fig. 5(b) for blend Y. The J vs. Δa curve for isotropic X is shown in Fig. 6(a). For the blends, the J values were plotted against the length of the stress-whitened zone, Δl, instead of crack growth length, Δa. The J vs. Δl is composed of two lines with different slopes as shown in Fig. 6(b) and (c) for Y and Z, respectively. Initially, the J increased less rapidly, indicating that the applied energy is dissipated in the sample through the formation of the damaged zone at the crack tip. Subsequently, the slope increased after crack initiation because the energy is now consumed by two processes; crack growth and formation of a damage zone ahead of the crack tip. The intersection of these two lines can be regarded as defining the onset of crack growth. This procedure gave a J_{IC} (not $J_{0.2}$) value for the blends Y and Z. This method of plotting J against Δl has been used by other workers [20,27,49] for cases where the conventional approach of plotting J vs. Δa was not possible. To demonstrate the difference between Δa and Δl, a sample of blend Y was loaded until crack growth was visible, on the surface, by naked eye. The sample was unloaded with a spacer and polished half way through the thickness to remove the skin and reveal the crack growth. The side view of the sectioned sample showed

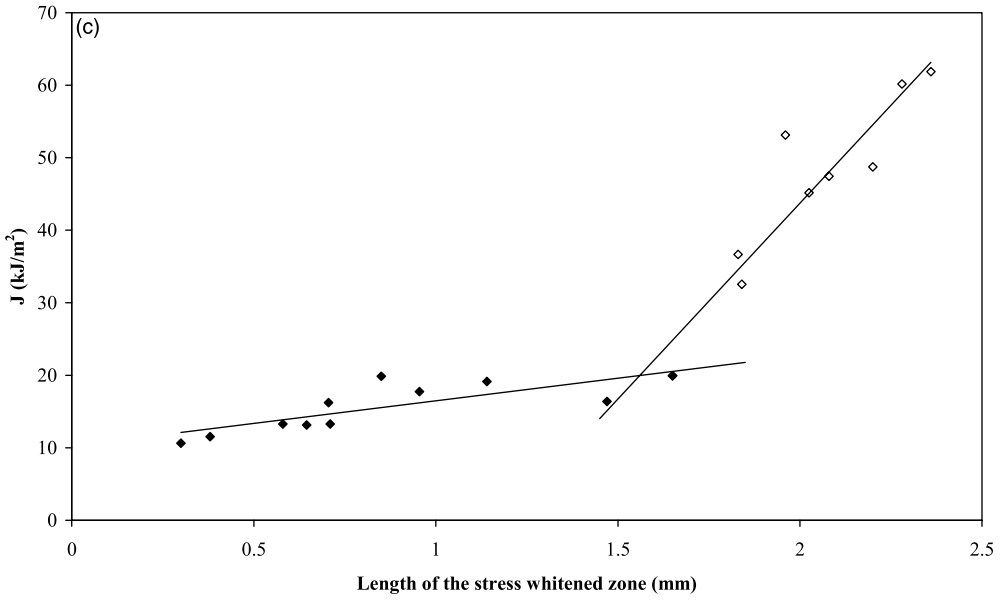

Fig. 6 (*continued*)

clear evidence of the presence of the crack growth (Δa) and the damage zone (Δl) ahead of it is shown in Fig. 7.

In the isotropic state, adding 10% elastomer to the brittle semi-crystalline PET matrix showed a marked improvement in the fracture toughness for the following reasons. In the case of X (elastomer content = 0), additional constraints imposed by the neighbouring material raise the yield stress to a level comparable to the fracture stress of the material. As a result, the energy absorption is confined to a small volume just at the vicinity of the crack tip indicating that the amount of plastic energy absorbed is low. The addition of 10% elastomer to the brittle PET matrix relieves the constraint at the crack tip by reducing the yield stress of the material. This reduction in constraint by rubber toughening facilitates more neighbouring material to participate in the yielding process. It is widely accepted that the role of the elastomer particles is to relieve the constraint at the crack tip by inducing shear yielding and/or multiple crazing in the matrix. The formation of cavities within the rubber particles and debonding from the parent matrix are also understood to contribute to the enhancement of toughness in the blends [50].

The toughness of the isotropic X, Y and Z from the J vs. Δa and J vs. Δl plots are presented in Table 1. The compatibilized blend (Z) has higher toughness than the homopolymer (X) and the non-compatibilized blend (Y). By comparing the shape of the crack front of X, Y and Z (Fig. 4(a)–(c)), it is clearly evident that grafting the elastomer with GMA before blending with the parent polymer produces the maximum crack blunting i.e. the crack initiation was delayed to much higher strains as confirmed in Fig. 3. Even though the yield stress of the blends is lower, delaying the fracture process to higher strain is the main factor of the toughness enhancement of the blends. It was shown earlier in part 1 of this series that adding a grafted elastomer finely disperses the elastomer particles in the PET matrix reduces the interparticle distance compared to the case where the elastomer is not grafted. This reduction in the interparticle distance contributes to the increased toughness [51] of the blend Z, when compared to the case where the elastomer is not grafted (Y).

3.2. Fracture behaviour of die-drawn (DD) and roll-drawn (RD) X, Y and Z with the initial notch parallel to the draw direction (PL)

For a draw ratio of 3.2, the fracture behaviour of

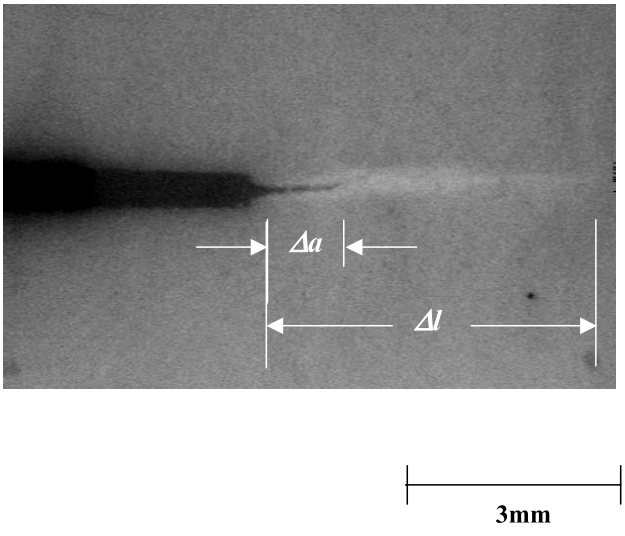

Fig. 7. Side view of polished isotropic Y (10 wt% mPE) showing crack growth (Δa) and the damage zone (Δl) ahead of the crack tip. The direction of crack propagation is from left to right.

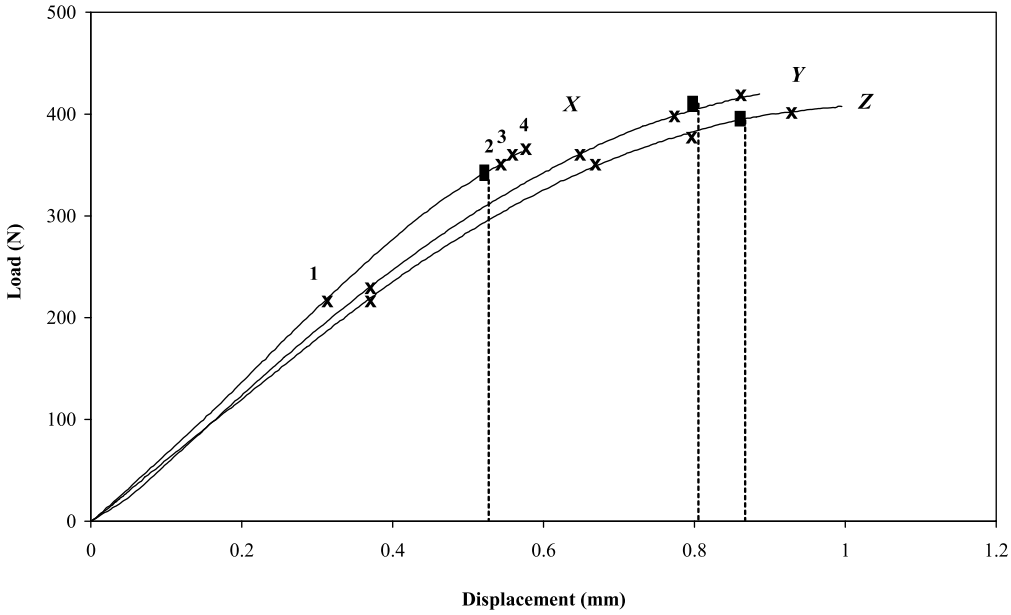

Fig. 8. Load-displacement plots with crack initiation points (■) for DD X-PL, DD Y-PL and DD Z-PL for $R_A = 3.2$.

roll-drawn X (PET), Y (10 wt% mPE) and Z (10 wt% GMA-mPE) was identical to that of the die-drawn samples and hence only one case will be discussed below. The load-displacement plots and the corresponding crack tip sequences during the fracture test on die-drawn X, Y and Z are shown in Figs. 8 and 9, respectively.

The load-displacement plot for DD X-PL remained linear up to point 1, with very little blunting of the crack tip (Fig. 9(a-1)). On further loading to point 2, the crack initiated in the damage zone at the vicinity of the crack tip (Fig. 9(a-2)). At point 3 (Fig. 9(a-3)), a discontinuous crack growth phenomenon as observed in isotropic X was seen to initiate. The cracks coalesced at point 4 (Fig. 9(a-4)) resulting in a drop in load.

For DD Y-PL and DD Z-PL (Fig. 8), the load-displacement curve deviated from the linear region at point 1 due to the formation of a plastic zone at the crack tip (Fig. 9(b-1) and (c-1)). Further loading to point 2 increased the size of the damage zone and the crack growth started at point 3 (Fig. 9(b-3) and (c-3)). Subsequent loading to higher displacements led to the stable crack growth inside the damage zone (Fig. 9(b-4) and (c-4)). The damage zone was much bigger in DD Z-PL, implying that more energy is absorbed in the damage zone i.e. more neighbouring material now participated in the fracture process. For the samples tested in this direction, the crack growth was clearly visible in the cold fractured surface.

The plot of J vs. Δa for X-PL, Y-PL and Z-PL is shown in Fig. 10(a)–(c) for both the roll-drawing and die-drawing processes. The $J_{0.2}$ values, obtained from these plots, are tabulated in Table 2. The results show that the toughness of the oriented samples ($R_A = 3.2$) from both the die-drawing and roll-drawing processes, when tested with the initial notch parallel to the draw direction (PL), decreased when compared to the isotropic material. In this direction, the compatibilized blend (Z-PL) was tougher than the drawn homopolymer (X-PL) and the non-compatibilized blend (Y-PL). It is interesting to note that the drawn blends (Y-PL and Z-PL) have a very large improvement in toughness when compared to the isotropic PET homopolymer even in this most unfavourable orientation.

In spite of the differences in processing, the samples drawn to a draw ratio of 3.2 using the die-drawing and roll-drawing processes yielded comparable toughness values. Similar conclusions have been reported for polypropylene

Table 1
J-integral fracture results on isotropic semi-crystalline PET homopolymer (X) and toughened blends (Y and Z)

Sample	$J_{0.2}$ (kJ/m^2)	J_{IC} (kJ/m^2)
X isotropic	10.2±0.6	–
Y isotropic	–	20.5±1.2
Z isotropic	–	27.0±1.7

Table 2
J-integral fracture results on the die-drawn (DD) and roll-drawn (RD) X, Y and Z with the initial notch parallel to the draw direction (PL)

Sample	$J_{0.2}$ (kJ/m^2)
DD X-PL	3.6±0.6
DD Y-PL	19.2±1.2
DD Z-PL	24.0±1.3
RD X-PL	5.1±0.5
RD Y-PL	19.2±0.8
RD Z-PL	19.6±0.9

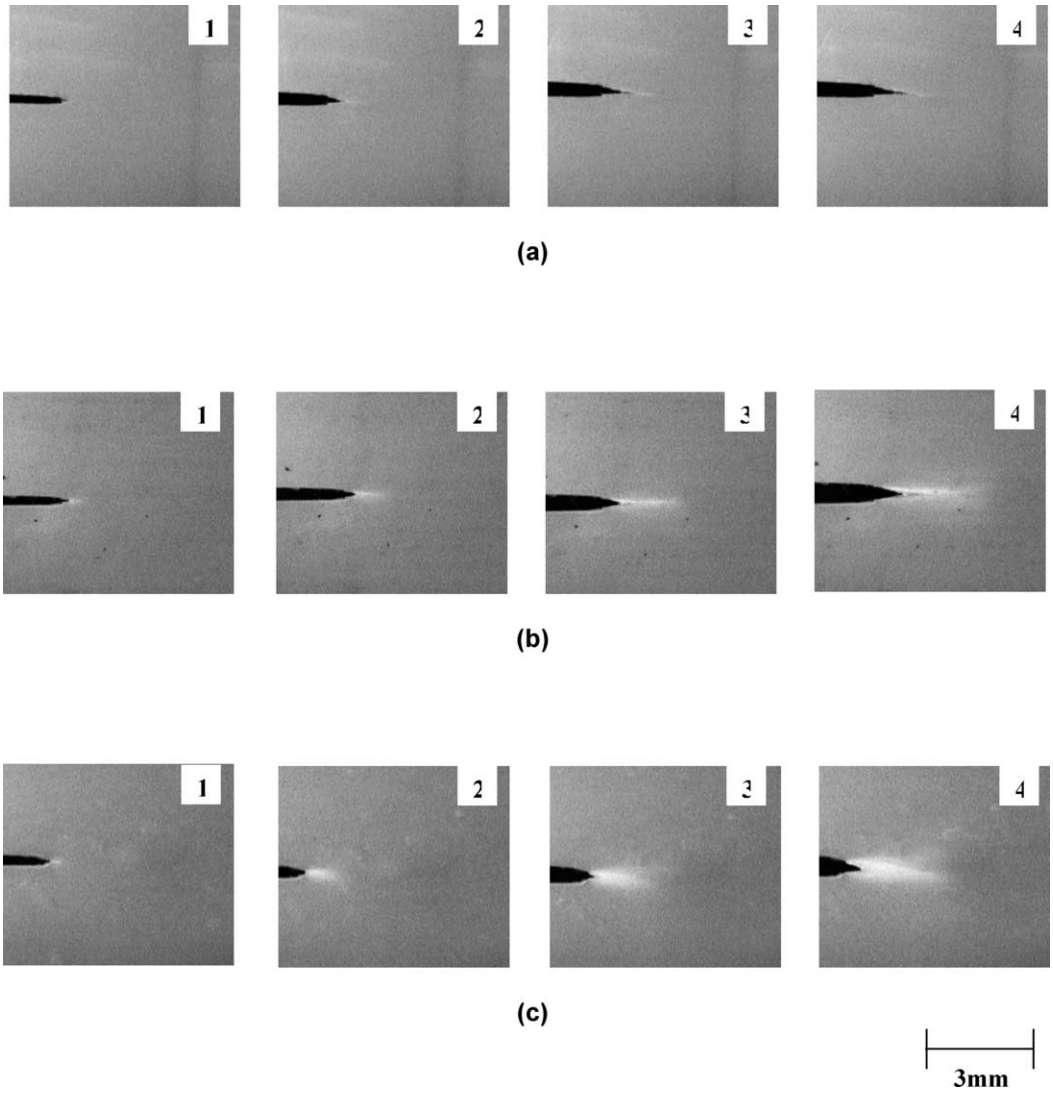

Fig. 9. Photographic sequence during the SENT test for (a) DD X-PL, (b) DD Y-PL and (c) DD Z-PL for $R_A = 3.2$ [(↔)-draw direction (↕)-test direction]. 1–4 in the inset of the photographs correspond to the points marked on the load-displacement curve shown in Fig. 8.

oriented by rolling and die-drawing [52] and for oriented toughened polypropylene produced by die-drawing and roll-drawing processes [53]. The small discrepancies in the toughness values between the die-drawn and roll-drawn sheets could be due to experimental imprecision or to minor differences in the processing conditions.

3.3. Fracture behaviour of die-drawn (DD) and roll-drawn (RD) X, Y and Z with the initial notch perpendicular to the draw direction (PR)

Similar to the results for the initial notch parallel to the draw direction, the fracture behaviour of samples drawn to a draw ratio of 3.2 and tested with the initial notch perpendicular to the draw direction was similar for die-drawn and roll-drawn samples. Hence the fracture behaviour of the materials produced only by the die-drawing process will be discussed in detail. The load-displacement curves for X (PET), Y (10 wt% mPE) and Z (10 wt% GMA-mPE) with crack initiation points and the photographs of the crack tip at specific points during the fracture test are shown in Figs. 11 and 12 respectively.

As shown in Fig. 12(a-1), when X oriented to a draw ratio of 3.2 was tested with the initial crack perpendicular to the draw direction (DD X-PR), two 'kidney' shaped yielded zones formed around the crack tip at the point where the curve deviated from the linear region in Fig. 11. Subsequent loading to point 2 in Fig. 11 increased the size of this yielded zone as the material in the vicinity of the crack tip appeared to be pulled in; this produced a dent in the fracture surface (Fig. 12(a-2)). The white region in the photographs is due to light reflections from the side and not as a result of stress whitening. Just before the beginning of the crack growth, point 2, a parabolic shaped damage zone caused by local

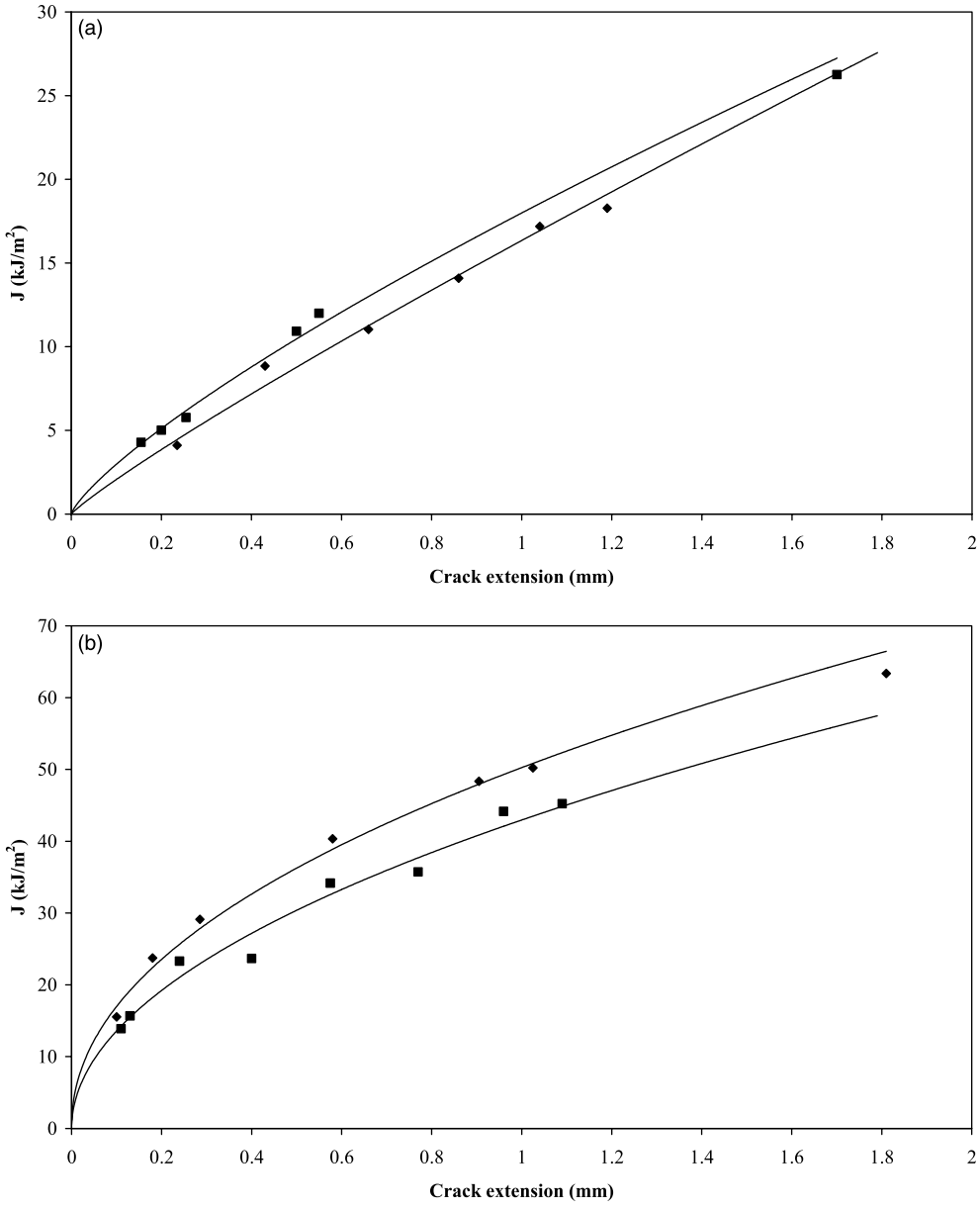

Fig. 10. (a) J vs. Δa curve for (♦) DD X-PL and (■) RD X-PL for $R_A = 3.2$. (b) J vs. Δa curve for (♦) DD Y-PL and (■) RD Y-PL for $R_A = 3.2$. (c) J vs. Δa curve for (♦) DD Z-PL and (■) RD Z-PL for $R_A = 3.2$.

delamination at the crack tip occurred in the yielded zone. This feature is marked with an arrow in Fig. 12(a-2) and can also be seen in the subsequent photographs in Fig. 12(a). The size of the delaminated zone at the crack tip remained constant in size as the crack propagated stably through the damaged zone. Thereafter (Fig. 12(a-3) and (a-4)), the growth of the crack happened stably in this damage zone. In this case the crack tip was highly constrained by the surrounding material.

In the case of the drawn blend DD Z-PR (Fig. 12(c)), the size of the plastic zones was much bigger when compared to that of DD X-PR and DD Y-PR. Stable crack growth occurred at point 2 after initial blunting between point 1 and point 2. The delamination ahead of the crack tip was not seen in the oriented blends because of the opacity of the samples. It has been shown earlier, in part 1 of this series, that the yield stress (on unnotched samples) of all the three materials along the draw direction increases with draw ratio and that blending with 10% elastomer causes a drop in yield stress. This could reduce the constraint at the crack tip and permit more neighbouring material to participate in the yielding process. In the case of X (elastomer content = 0), the additional constraint imposed by the neighbouring material raises the yield stress to a level comparable to the

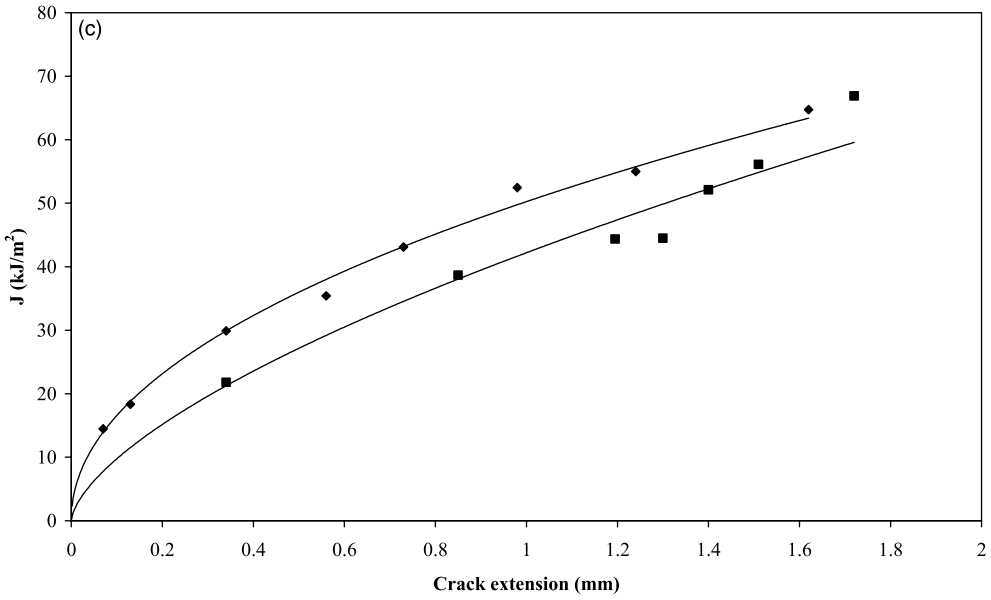

Fig. 10 (*continued*)

fracture stress of the material. As a result, the energy absorption is confined to a small volume just at the vicinity of the crack tip.

The crack front was not visible in the blend Z-PR from the die-drawing and roll-drawing processes and hence the J in this case was plotted against the size of the damage or stress whitened zone, Δl. The J vs. Δa curves for X-PR and Y-PR and the J vs. Δl plot for Z-PR for both roll-drawing and die-drawing processes are shown in Fig. 13(a)–(d), respectively, and the results from the above plots are summarised in Table 3.

Comparing the results in Table 3 with those in Table 1, it can be seen that the homopolymer and the blends showed a considerable improvement in the toughness over the isotropic material. For both orientation processes, the homopolymer (X-PR) exhibited higher toughness than the blends (Y-PR and Z-PR). The toughness in this direction depends on the molecular orientation in the base polymer. In

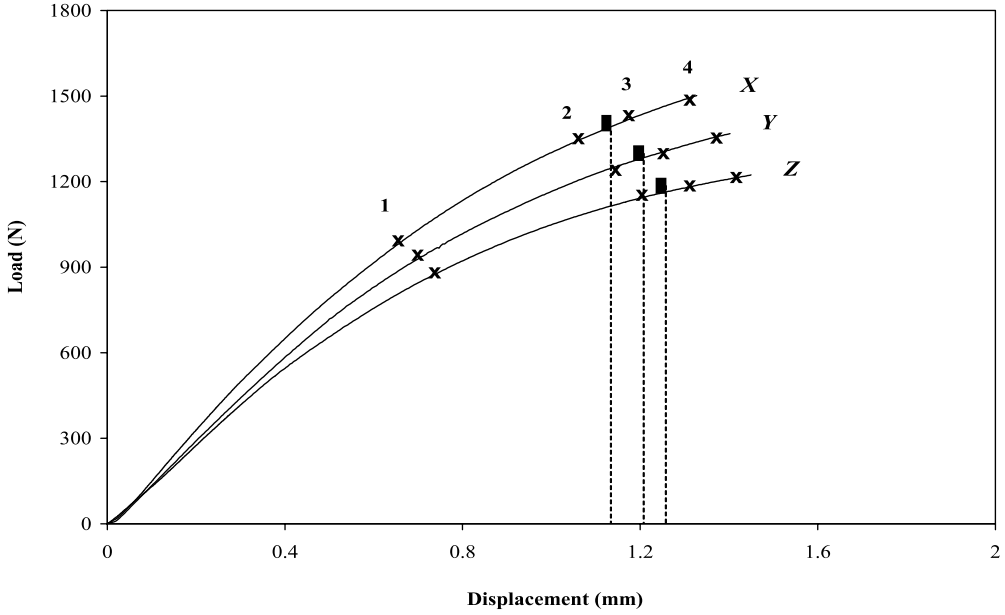

Fig. 11. Load-displacement plots with crack initiation points (■) for DD X-PR, DD Y-PR and DD Z-PR for $R_A = 3.2$.

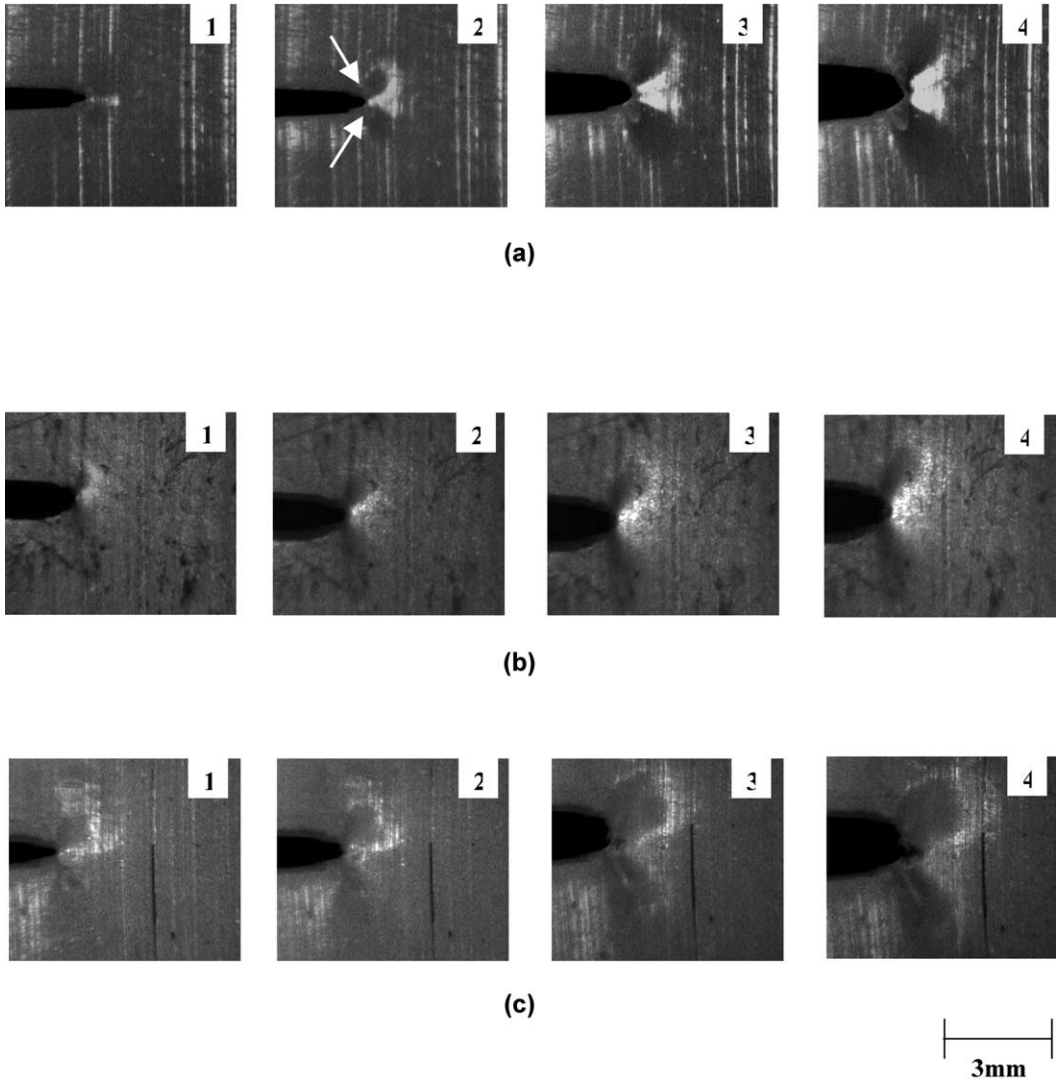

Fig. 12. Photographic sequence during the SENT test for (a) DD X-PR, (b) DD Y-PR and (c) DD Z-PR for $R_A = 3.2$ [(↕)-draw direction (↕)-test direction]. 1–4 in the inset of the photographs correspond to the points marked on the load-displacement curve shown in Fig. 11.

part 1 of this series, from the FTIR and modulus results, we reported that the molecular orientation of the PET increased with draw ratio and the addition of the elastomer phase inhibited the molecular orientation in the PET matrix. Thus although the crack initiated in X-PR before it did in the blends Y-PR and Z-PR (Fig. 11), the fracture stress of oriented X was higher than for the blends. The reduced toughness of the oriented blends relative to an unfilled material can be attributed to the decrease in molecular orientation in the blends and hence reduction in fracture stress.

As reported earlier in part 1 of this series, the molecular orientation of PET from the roll-drawing and die-drawing processes is similar for identical draw ratios. Since the toughness in this direction depends on the molecular orientation in PET and because the samples from the two processes have identical molecular orientation, their toughness is also identical.

Table 3
J-integral fracture results on the die-drawn (DD) and roll-drawn (RD) X, Y and Z with the initial notch perpendicular to the draw direction (PR)

Sample	$J_{0.2}$ (kJ/m^2)	J_{IC} (kJ/m^2)
DD X-PR	202±5	–
DD Y-PR	127±4	–
DD Z-PR	–	89±6
RD X-PR	215±4	–
RD Y-PR	133±5	–
RD Z-PR	–	90±4

4. Conclusions

We have investigated the fracture behaviour of isotropic and oriented poly(ethylene terephthalate) (PET) homopolymer, a blend containing 10% of polyethylene based

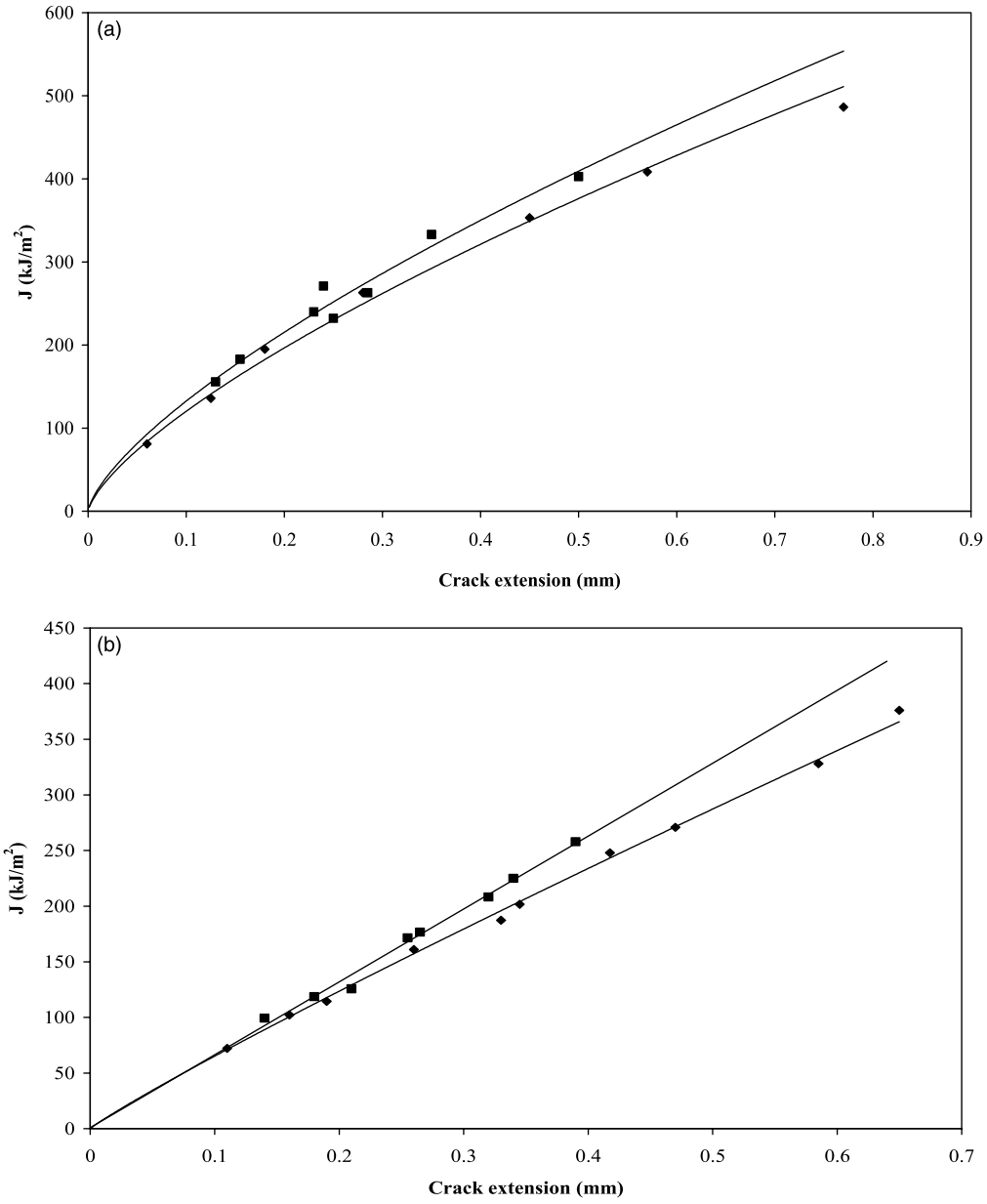

Fig. 13. (a) J vs. Δa curve for (♦) DD X-PR and (■) RD X-PR for $R_A = 3.2$. (b) J vs. Δa curve for (♦) DD Y-PR and (■) RD Y-PR for $R_A = 3.2$. (c) J vs. Δl curve for DD Z-PR for $R_A = 3.2$. (d) J vs. Δl curve for RD Z-PR for $R_A = 3.2$.

elastomer and a blend containing 10% of compatibilized elastomer. The homopolymer and the blends were oriented to a draw ratio of 3.2 using two solid-state orientation processes: die-drawing and roll-drawing. In the isotropic state, the compatibilized blend had a higher toughness than the homopolymer and the non-compatibilized blend. The oriented sheets, from the die-drawing and roll-drawing processes, were tested with the initial notch both parallel and perpendicular to the draw direction. For the former case, the toughness decreased compared to the isotropic material. The drawn blends, in this direction, have a very large improvement in toughness compared to the isotropic PET homopolymer. The compatibilzed blend was tougher than the homopolymer and the non-compatibilized blend. When tested with the initial notch perpendicular to the draw direction, the homopolymer and the blends showed a considerable improvement in toughness over the isotropic homopolymer and blends. The toughness in this direction is dependent on the degree of orientation in PET. Addition of elastomer reduced the degree of molecular orientation in the PET and thus the drawn homopolymer, in this direction, was tougher than the blends. For similar draw ratios, the toughness of the oriented sheets, both parallel and perpendicular to the draw direction, obtained from the die-drawing and roll-drawing processes were nearly identical.

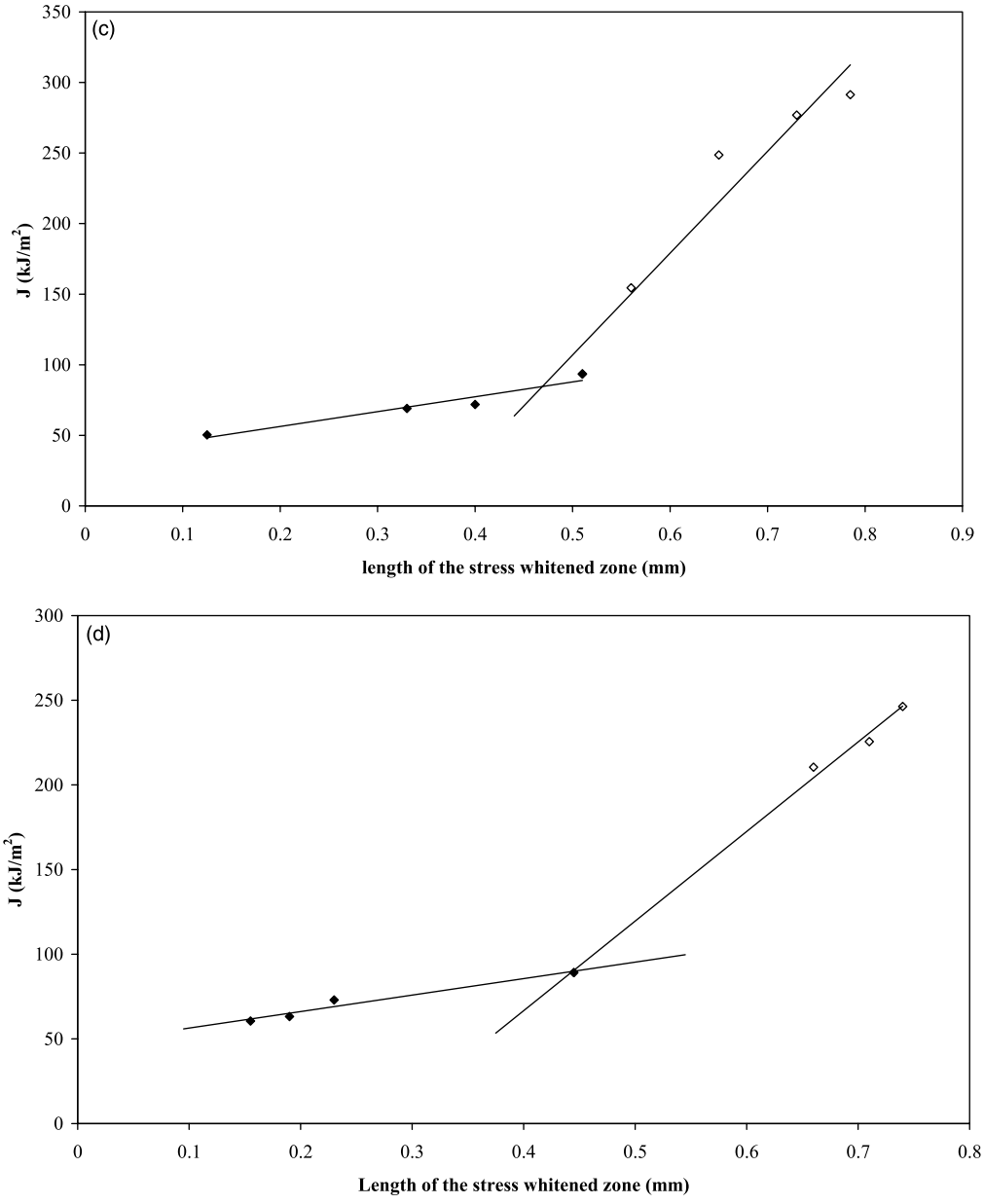

Fig. 13 (*continued*)

References

[1] Mohanraj J, Chapleau N, Ajji A, Duckett RA, Ward IM. J Appl Polym Sci 2003;88:1336–45.
[2] Bucknall CB. Toughened plastics. London: Applied Science Publications; 1977.
[3] Yee AF, Du J, Thouless M. Designing toughened plastics through the control of morphology and properties of toughened phase, ANTEC Conference Proceedings, New York, 1990.
[4] Michler GH. Polym Adv Tech 1998;9:812–22.
[5] Van der Wal A, Nijhof R, Gaymans RJ. Polymer 1999;40:6031–44.
[6] Bucknall CB, Clayton D, Keast WE. J Mater Sci 1972;7:1443–53.
[7] Bucknall CB, Clayton D, Keast WE. J Mater Sci 1973;8:514–24.
[8] Wu JS, Mai YW. Mater Forum 1995;19:181–99.
[9] Van der Wal A, Gaymans RJ. Polymer 1999;40:6067–75.
[10] Hashemi S. Plast Rubb Comp Proc Appl 1993;20:229–37.
[11] Karger-Kocsis J, Moskala EJ, Shang PPJ. Therm Anal Cal 2001;63: 671–8.
[12] Arkhireyeva A, Hashemi S. J Mater Sci 2002;37:3675–83.
[13] Stearne JM, Ward IM. J Mater Sci 1969;4:1088–96.
[14] Foot JS, Ward IM. J Mater Sci 1972;7:367–87.
[15] Foot JS. PhD Thesis, University of Bristol, 1972.
[16] Pecorini TJ, Hertzberg RW. Polymer 1993;34:5053–62.
[17] Mai YW, Cotterell B. Int J Frac 1986;32:105–25.
[18] Hill R. J Mech Phys Solids 1952;4:19–30.
[19] Narisawa I, Takemori T. Polym Eng Sci 1989;29:671–8.
[20] Hornsby PR, Premphet K. J Mater Sci 1997;32:4767–75.
[21] Riew CK, Kinloch AJ, editors. Toughened plastics: science and engineering. Washington: American Chemical Society; 1993.
[22] Savadori A, Bramuzzo M, Marega C. Polym Test 1984;4:73–89.
[23] Hashemi S, Williams JG. J Mater Sci 1991;26:621–30.
[24] Lu ML, Chiou KC, Chang FC. Polymer 1996;37:4289–97.

[25] Parker DS, Sue HJ, Huang J, Yee AF. Polymer 1990;31:2267–77.
[26] Hashemi S, Williams JG. Polym Eng Sci 1986;26:760–7.
[27] Lee CB, Chang FC. Polym Eng Sci 1992;32:792–803.
[28] Kim BH, Joe CR. Polym Test 1987;7:355–63.
[29] Kim BH, Joe CR, Otterson DM. Polym Test 1989;8:119–30.
[30] Ha CS, Kim Y, Lee WK, Cho WJ. J Appl Polym Sci 1994;51:1381–8.
[31] Ha CS, Kim Y, Lee WK, Cho WJ. Polymer 1998;39:4765–72.
[32] Arkhireyeva A, Hashemi S. Plast Rubber Compos 2001;30:337–50.
[33] Bernal CR, Montemartini PE, Frontini PM. J Polym Sci, Polym Phys 1996;34:1869–80.
[34] Morhain C, Velasco JI. J Mater Sci 2001;36:1487–99.
[35] Zhou J, Yin JH, Liu WL, Li BY. Polym Commun 1991;32:423–5.
[36] Martinatti F, Ricco T. Polym Test 1994;13:405–18.
[37] Ramsteiner F. Polym Test 1999;18:641–7.
[38] Crouch BA, Huang DD. J Mater Sci 1994;29:861–4.
[39] Seidler S, Grellmann W. J Mater Sci 1993;28:4078–84.
[40] Grellmann W, Seidler S, Hesse W. Testing of plastics, laboratory manual. Wittenburg: Martin-Luther University; 2001.
[41] Seidler S, Grellmann W. Polym Test 1995;14:453–69.
[42] Polato F. J Mater Sci 1985;20:1455–65.
[43] Bramuzzo M. Polym Eng Sci 1989;29:1077–88.
[44] Rice JR. J Appl Mech 1968;35:379–86.
[45] Sumpter JDG, Turner CE. Int J Frac 1973;9:320–1.
[46] ASTM D6068-96, Annual book of ASTM standards 1996.
[47] Lu X, Qian R, Brown N. J Mater Sci 1991;26:917–24.
[48] O'Connell PA, Bonner MJ, Duckett RA, Ward IM. Polymer 1995;36: 2355–62.
[49] Zhang MJ, Zhi FX, Su XR. Polym Eng Sci 1989;29:1142–6.
[50] Paul DR, Bucknall CB, editors. Polymer blends. Performance, vol. 2. New York: John Wiley; 2000.
[51] Wu S. J Appl Polym Sci 1988;35:549–61.
[52] Chaffey CE, Taraiya AK, Ward IM. Polym Eng Sci 1997;37:1774–84.
[53] Mohanraj J, Chapleau N, Ajji A, Duckett RA, Ward IM. unpublished results.